Zhu S and Zhang Y (2013) Loading rate effect on superelastic SMA-based seismic response modification devices. *Earthquakes and Structures*. Accepted.

Loading rate effect on superelastic SMA-based seismic response modification devices

Songye Zhu[1,2,*] and Yunfeng Zhang[3]

1. The Hong Kong Polytechnic University Shenzhen Research Institute, Shenzhen 518057, China

2. Department of Civil and Environmental Engineering, The Hong Kong Polytechnic University, Hong Kong

3. Department of Civil and Environmental Engineering, University of Maryland, College Park, MD 20742, USA

ABSTRACT

The application of shape memory alloys (SMAs) to the seismic response reduction of civil engineering structures has attracted growing interest due to their self-centering feature and excellent fatigue performance. The loading rate dependence of SMAs raises a concern in the seismic analysis of SMA-based devices. However, the implementation of micromechanics-based strain-rate-dependent constitutive models in structural analysis software is rather complicated and computationally demanding. This paper investigates the feasibility of replacing complex rate-dependent models with rate-independent constitutive models for superelastic SMA elements in seismic time-history analysis. Three uniaxial constitutive models for superelastic SMAs, including one rate-dependent thermomechanical model and two rate-independent phenomenological models, are considered in this comparative study. The pros and cons of the three nonlinear constitutive models are also discussed. A parametric study of single-degree-of-freedom systems with different initial periods and strength reduction factors is conducted to examine the effect of the three constitutive models on seismic simulations. Additionally, nonlinear time-history analyses of a three-story prototype steel frame building with special SMA-based damping braces are performed. Two suites of seismic records that correspond to frequent and design basis earthquakes are used as base excitations in the seismic analyses of steel-braced frames. The results of this study show that the rate-independent constitutive models, with their parameters properly tuned to dynamic test data, are able to predict the seismic responses of structures with SMA-based seismic response modification devices.

* Corresponding author. Assistant Professor. Email: ceszhu@polyu.edu.hk; Tel: (+852) 3400 3964;

Keywords: shape memory alloy, superelasticity, loading rate effect, damper, constitutive model

1. INTRODUCTION

As a promising smart material, shape memory alloys (SMAs) have attracted growing interest in the seismic protection of civil engineering structures. Studies on SMA-based seismic response modification devices were reported by Grasser and Cozzarelli (1991), Aiken et al. (1993), Whittaker et al. (1995), Clark et al. (1995), Dolce et al. (2000), DesRoches et al. (2004), Dolce et al. (2005), McCormick et al. (2006), Zhu and Zhang (2007a), Li et al. (2008), Casciati et al. (2009), Padgett et al. (2010), Yang et al. (2010), Liu et al. (2011), and several other researchers. The self-centering and energy-dissipating capabilities of superelastic SMAs make these materials advantageous in seismic response control of structures. For example, Dolce et al. (2005) validated the benefits of SMA-incorporated base isolations in controlling structural and non-structural damage of RC frames. Padgett et al. (2010) tested SMA restrainer cables on a four-span large-scale concrete bridge. The shaking table test results showed that the cables effectively reduced the unseating risk of the bridge deck. Casciati et al. (2009) proposed a passive SMA device for highway bridges, and demonstrated its ability to control the peak displacement response. Wilson and Wesolowsky (2005), Song et al. (2006), and Ozbulut et al. (2011) provided comprehensive reviews on the applications of SMAs in civil engineering. Due to the nature of stress-induced martensitic transformation of superelastic SMAs, the applications of these materials are generally uniaxial in order to obtain maximum recoverable deformation.

Loading rate dependence is a property of concern for a variety of materials (e.g. Kim et al. 2008; Kozar and Ozbolt 2010). Several experimental findings suggest that different loading rates generally lead to variation in hysteretic and thermal behaviors of SMAs (Prahlad and Chopra 2003; Zhu and Zhang 2007b). The rate-induced thermomechanical effect of SMAs has drawn attention in seismic applications, wherein the dynamics of SMA-based energy dissipation devices and structures is of interest. Rate-dependent thermomechanical constitutive models for SMA were studied by researchers (e.g., Prahlad and Chopra 2003; Boyd and Lagoudas 1998; Auricchio et al. 1999, 2006; Zhu and Zhang 2007b; Monteiro et al. 2010). These thermomechanical constitutive models are able to satisfactorily reproduce hysteretic

behavior of SMA materials under varying loading rates. However, most rate-dependent constitutive models for SMAs are derived in a thermodynamics framework. The associated complexity of this process deters engineers from using these models in seismic applications of SMAs. Furthermore, rate-dependent constitutive models for SMAs cannot be directly used in nonlinear static analysis procedures such as pushover analyses, despite the fact that these models are able to provide accurate and reliable results in nonlinear dynamic analyses. On the other hand, rate-independent phenomenological models for SMAs have been developed (e.g., Graesser and Cozzarelli 1991). Temperature and loading rate effects are not explicitly considered in these rate-independent models for SMA. However, these models are appealing in seismic analyses because of their simpler mathematical expression and less computational demand compared to thermomechanical constitutive models.

Thus, this paper presents a feasibility study on the use of rate-independent constitutive models for superelastic SMAs in seismic response analyses of structures equipped with SMA-based devices through a comparative study of three nonlinear constitutive models. The constitutive models considered in this study for superelastic SMA wires are as follows: (i) a rate-dependent thermomechanical model; (ii) a rate-independent phenomenological model termed modified Wilde model; and (iii) a piecewise-linear flag-shaped model. A parametric study of single-degree-of-freedom (SDOF) systems with superelastic SMA elements is conducted with varying initial elastic periods and strength reduction factors. Results of the nonlinear dynamic analysis of a three-story braced-frame building with SMA-based damping devices are also presented in this article.

2. LOADING RATE EFFECT ON SUPERELASTIC SMA

SMAs can exhibit two distinctive behavior at different ambient temperatures: shape memory effect and superelastic effect. Both these effects occur as a result of solid–solid phase transformations between the austenite and martensite. For example, an SMA exhibits superelastic behavior at ambient temperature $T>A_f$, where A_f is termed austenite finish temperature above which the microstructure of the SMA is fully austenitic. For an austenitic SMA, the phase transformation from austenite to martensite can be induced

either by reducing the ambient temperature or by applying stress; the stress-induced phase transformation is often referred to as superelastic behavior of the SMA. In superelasticity, the martensite phase is stable only at the presence of externally applied load, and reverse transformation takes place upon unloading. The material will return to its original undeformed shape after fully unloading (Grasser and Cozzarelli 1992). Among various SMAs, Nitinol is the most widely used because of its superior mechanical properties, such as high ductility, high corrosion resistance, and excellent high- and low-cycle fatigue performance. For example, the maximum recoverable strain of superelastic Nitinol can reach up to 8%, and its fatigue life under 8% strain cyclic loading can go over 2,000 cycles (Zhu and Zhang 2008). These favorable properties and its self-centering and energy dissipating capability make Nitinol-based energy dissipation devices very promising in seismic applications.

The writers tested superelastic Nitinol wires with a diameter of 0.58 mm (0.025 in) and a gauge length of 254 mm (10 in) on an MTS universal testing machine at a room temperature of 23 ºC. The Nitinol wires were preloaded for 80 cycles before the formal wire testing to stabilize their hysteretic behavior. The hysteresis became repeatable after preloading, and no apparent residual strain and degradation of strength occurred in the subsequent cyclic tests. Fig. 1 shows the stress–strain curves of the superelastic Nitinol wires from the uniaxial quasi-static and dynamic tensile tests with loading periods of 0.25, 0.5, 2, and 10 s (equivalent to loading frequencies 4, 2, 0.5, and 0.1 Hz, respectively). The loading rates in this study are defined by loading periods instead of loading frequencies because the former are more frequently used in seismic response spectra. The loading periods of the dynamic tests (i.e., from 0.25 s to 10 s) are the typical range of interest in earthquake engineering. The Nitinol wires were cyclically loaded at a constant strain amplitude of 6% for each loading frequency. Figs. 1(a) and 1(b) show the stress–strain curve in the 1^{st} and 10^{th} cycles, respectively, for different loading rates.

Fig. 1 shows that the slopes of the upper (loading) and lower (unloading) plateaus of the stress–strain curve are essentially flat for the quasi-static test data. Compared with the quasi-static test results, the slopes of the loading and unloading plateaus in the dynamic tests with the loading periods from 0.25 s to 10 s become larger, whereas the amount of energy dissipation (i.e., the enclosed area in each cycle)

becomes smaller. The slopes of the loading/unloading plateau are commonly referred as "post-yield" stiffness in earthquake engineering; however, in actuality, phase transformation, rather than yielding, takes place in SMAs. The increased slopes, which are often considered a favorable effect in seismic applications, are caused by self-heating phenomena resulting from latent heat. The austenite to martensite transformation in the loading path is exothermic, whereas the martensite to austenite transformation in the unloading path is endothermic. Temperature fluctuation in quasi-static tests is nearly negligible due to the heat transfer between the SMA wires and the surrounding environment. However, the heat transfer is limited in each cycle under a fast loading rate. Thus, the loading path is accompanied by a rise in wire temperature, whereas temperature drops in the unloading path. The transformation stress of SMAs typically becomes higher with increasing temperature (Liang and Rogers 1990). In the dynamic tests, the temperature variation in each cycle leads to the increased value of "post-yield" stiffness ratio, whereas a relatively flat transformation plateau is observed in the quasi-static tests.

Fig. 1(a) shows that only slight differences exist among these hysteretic loops corresponding to the 1st cycle of the dynamic tests, especially for loading periods from 0.25 s to 2 s. Fig. 1(b) shows that differences among the hysteretic loops of the tenth cycles can be clearly observed. This figure illustrates that the hysteretic shapes are usually unstable in the first several cycles under dynamic loading. Compared with the 1st cycle, the hysteretic loops in the 10th cycle shift downwards for the loading periods of 2 and 10 s, whereas the hysteretic loop shifts upwards for the loading period of 0.25 s. The hysteretic loops of the 1st and 10th cycles are nearly identical for the loading period of 0.5 s and the quasi-static loading. The energy dissipation capacity is slightly reduced with the increasing number of loading cycles. The 10th cycle hysteretic loop is quite stable and repeatable in the subsequent cycles, except for the loading period of 0.25 s. More cycles are required to reach stable hysteretic loops under the loading period of 0.25 s; as a result, the upward shift was still observe after the 10th loading cycle.

In addition to the temperature variation of Nitinol wires within each cycle, temperature also varies from cycle to cycle. Energy equilibrium requires the absorbed specific heat to be equal to the latent heat generation and mechanical energy dissipation, subtracted by the heat loss to the environment (Zhu and

Zhang 2007b). After a full loading–unloading cycle, Nitinol returns to the austenite state, and the latent heat generation is approximately zero. If the heat generated by mechanical energy dissipation differs from the heat loss in one cycle, the temperature at zero strain will be different at the start and end moments of this particular cycle. This variation of zero-strain temperature shifts the hysteretic loops with the increasing number of loading cycles until the mechanical energy dissipation is equal to the heat loss in one cycle and the temperature cycles stabilize. In general, heat loss to the environment in one cycle becomes smaller with the increase of loading rate. The wire test results in Fig. 1 show that the zero-strain temperature drops in the first several cycles for loading periods of 2 and 10 s, and rises for the loading period of 0.25 s; however, it does not significantly change for the loading period of 0.5 s. The different variation trends of zero-strain temperature leads to the different shifting pattern of the hysteretic loops in the dynamic tests of SMA wires.

These findings suggest that the thermomechanical effect of superelastic Nitinol wires should be carefully evaluated for nonlinear dynamic analyses because some important material properties of Nitinol, such as the "post-yield" stiffness, "yield" strength, and energy dissipation, vary with loading rates. Thus, the influence of these rate-dependent material properties on seismic response of structures equipped with SMA-based energy dissipating devices are investigated in this study.

3. CONSTITUTIVE MODEL OF SUPERELASTIC SMA WIRE

A constitutive law that accurately describes the stress–strain relationship of superelastic SMA wires should be developed to incorporate effectively the SMA-based damping devices into the design of actual structures. The mechanical behavior of SMAs is usually modeled from either a phenomenological or a micromechanical approach (Brocca et al. 2002). Phenomenological models are often *ad hoc* descriptions aimed at fitting experimental data, and are usually accurate in predicting the uniaxial response of SMAs. In general, phenomenological models are less complicated and less computationally demanding than are micromechanics-based models. Three phenomenological constitutive models are considered for superelastic SMA wires in this study: (i) a rate-dependent thermomechanical model; (ii) a rate-

independent phenomenological model termed modified Wilde model; and (iii) a rate-independent piecewise-linear flag-shaped model. These models are briefly described in the following sections.

3.1 Rate-dependent thermomechanical constitutive model (TM model)

Zhu and Zhang (2007b) proposed an improved uniaxial thermomechanical constitutive model that is able to predict the strain-rate-dependent behaviors of superelastic SMA wires, including temperature variation, transformation stress, "post-yield" stiffness, and energy dissipation. This rate-dependent phenomenological constitutive model was derived for cases with constant and non-constant elastic modulus within a thermodynamics framework using Helmholtz free energy density. The rate-dependent constitutive model consists three key components: a mechanical law, an energy balance equation, and a transformation kinetics rule. The rate form of this constitutive model and the corresponding implementation scheme with no iteration were presented by Zhu and Zhang (2007b). This model is not elaborated in this paper due to its complexity.

Table 1 provides the parameters of the TM model used to simulate the superelastic behavior of Nitinol wires in this study, where E_A and E_M represent the Young's modulus of the austenite and martensite states respectively, which are generally not equal. The transformation temperatures M_s, M_f, A_s and A_f refer to martensite start temperature, martensite finish temperature, austenite start temperature, and austenite finish temperature, respectively. The material constants c_A and c_M define the relation between the transformation stress and temperature. The latent heat of phase transformation and specific heat of material are denoted by L and C_p, respectively; k is the heat transfer coefficient; and ε_l is the maximum residual strain. Fig. 2 presents the experimental and simulation results of the stress–strain curves of superelastic Nitinol wires under four dynamic loading rates. The arrows in figure indicate the shift directions of the hysteretic loops with the increasing number of loading cycles. This TM model is able to predict the superelastic behavior of Nitinol wires for a variety of loading rates (Zhu and Zhang 2007b). This model is also able to capture two major thermomechanical behaviors of superelastic Nitinol wires under varying loading rates, namely, the increased slopes of transformation plateau under dynamic

loading rates and the shifting of hysteretic loops with the increasing number of loading cycles. Both loading rates are due to the thermal effect in superelastic Nitinol wires under dynamic loading.

3.2 Modified Wilde model (MW model)

Zhang and Zhu (2006) presented a modified version of a uniaxial phenomenological model for SMA wires. This model was initially developed by Grasser and Cozzarelli (1991), and was extended by Wilde et al. (2000) to include the hardening behavior of SMA materials after complete transition from austenite to martensite. The Wilde model was further modified by Zhang and Zhu (2006) to achieve better agreement with experimental results. The MW model is expressed as follows:

for the loading stage, $\dot{\varepsilon} > 0$

$$\begin{cases} \dot{\sigma} = E \cdot \left[\dot{\varepsilon} - \dot{\varepsilon} \cdot (\dfrac{\sigma - \beta}{Y})^n \right] \cdot u_I(\varepsilon) + E_m \cdot \dot{\varepsilon} \cdot u_{II}(\varepsilon) + (E_y \dfrac{\varepsilon_m - \varepsilon}{\varepsilon_m - \varepsilon_1} + E_m \dfrac{\varepsilon - \varepsilon_1}{\varepsilon_m - \varepsilon_1}) \cdot \dot{\varepsilon} \cdot u_{III}(\varepsilon) \\ \beta = \alpha \cdot E \cdot \varepsilon_{in} \end{cases} \tag{1a}$$

for the loading stage, $\dot{\varepsilon} < 0$

$$\begin{cases} \dot{\sigma} = E \cdot \left[\dot{\varepsilon} + \dot{\varepsilon} \cdot \mathrm{H}(\varepsilon_{in}) \cdot \mathrm{sgn}(\sigma - \beta) (\dfrac{|\sigma - \beta|}{Y})^n \right] \\ \beta = \alpha \cdot E \cdot [\varepsilon_{in} + f_T \cdot g(a\varepsilon_{in} + b)] \end{cases} \tag{1b}$$

where

$$g(t) = 1 - e^{-t^2} \tag{1c}$$

$$K = \begin{cases} 1 & \text{if } \varepsilon\dot{\varepsilon} > 0, \text{loading} \\ \mathrm{H}(\varepsilon_{in}\varepsilon) & \text{if } \varepsilon\dot{\varepsilon} \le 0, \text{unloading} \end{cases} \tag{1d}$$

$$u_I(\varepsilon) = 1 - u_{II}(\varepsilon) - u_{III}(\varepsilon) \tag{1e}$$

$$u_{II}(\varepsilon) = \begin{cases} 1 & \text{if } \varepsilon\dot{\varepsilon} > 0 \text{ and } |\varepsilon| \ge \varepsilon_m \\ 0 & \text{otherwise} \end{cases} \tag{1f}$$

$$u_{III}(\varepsilon) = \begin{cases} 1 & \text{if } \varepsilon \cdot \dot{\varepsilon} > 0 \text{ and } \varepsilon_1 < |\varepsilon| < \varepsilon_m \\ 0 & \text{otherwise} \end{cases} \tag{1g}$$

Here, σ and ε are the one-dimensional stress and strain, respectively; β is the one-dimensional backstress; E_A and E_M are the Young's modulus of the austenite and the martensite respectively; Y is the upper

"yielding" stress; α=E_y/(E-E_y) is a constant that governs the "post-yield" stiffness; material constants f_T, a, and b control the recovery of the inelastic strain upon unloading; n is a constant that controls the transition sharpness; sgn(·) is the Signum function; H(·) is unit step function (i.e., Heaviside function); and $\varepsilon^{\text{in}} = \varepsilon - \sigma / E$ is the inelastic strain.

Fig. 3(a) shows the stress–strain curve of superelastic Nitinol wires from the test data and the MW model, where the test data corresponds to a loading period of 0.5 s. Table 1 shows the model parameters adopted in this study. No apparent shift of hysteretic behavior could be observed at the loading period of 0.5 s with the increasing number cycles. The test data were thus selected to calibrate the parameters of the rate-independent constitutive model. The MW model agrees with the experimentally obtained hysteretic loops at different strain amplitudes. However, the MW model tends to slightly overestimate the energy dissipation in large strain cycles. Notably, the MW model is a rate-independent constitutive model.

3.3 Flag-shaped model (FS model)

The piecewise-linear flag-shaped hysteretic model has been widely used in the studies on self-centering seismic resisting systems, such as rocking walls, post-tensioned concrete or steel frames, and SMA devices, because of its simplicity (e.g., Christopoulos et al. 2002; Seo and Sause 2005; Mao and Li 2005; Andrawes and DesRoches 2005). A typical FS model that describes the stress–strain relationship of superelastic Nitinol wires can be fully defined by six parameters: elastic modulus of austenite E_A, elastic modulus of martensite E_M, "yield" stress σ_y, "post-yield" stiffness coefficient α, energy dissipation coefficient β, and transformation finish strain ε_M (Fig. 4). Fig. 3(b) plots the stress–strain curves of superelastic Nitinol wires from the test data and the FS model, wherein the test data correspond to a loading period of 0.5 s. The FS model is able to reasonably predict some key features of superelastic Nitinol wires, such as initial stiffness, "post-yield" stiffness, and upper and lower plateaus. However, apparent discrepancy can be observed between the test data and the prediction from the FS model on the unloading path, which leads to the overestimation of energy dissipation by the FS model.

The parameters of the MW and FS model are both tuned according to the dynamic test data instead of the quasi-static data. However, both models are rate-independent constitutive models.

4. PARAMETRIC STUDY: SDOF SYSTEM

A parametric study on nonlinear dynamic response of SDOF systems was conducted to compare the effect of different constitutive models on structural behavior under earthquakes. The resisting force of each SDOF systems was assumed to be solely provided by a superelastic Nitinol element.

4.1 Equation of motion

The governing equation of motion of a nonlinear SDOF system under seismic ground motion is

$$m \cdot \ddot{x} + c \cdot \dot{x} + F(x, \dot{x}) = -m \cdot \ddot{x}_g \tag{2}$$

where m is the mass; c is the viscous damping coefficient; x, $\dot{x}$, and $\ddot{x}$ are the relative displacement, velocity, and acceleration of the system, respectively; and $\ddot{x}_g$ is the ground acceleration. The nonlinear resisting force of the superelastic Nitinol element modeled using one of the aforementioned constitutive models is denoted by $F(x, \dot{x})$. The viscous damping ratio of the system was assumed to be 5% in this study.

The constitutive models presented in the previous section indicate that the parameters related to energy dissipation coefficient and the "post-yield" stiffness ratio were determined from the experimental results of the superelastic Nitinol wires. Thus, these variables were not examined in the parametric study. The two essential variables of the SDOF system are its initial elastic period T_0 and the strength reduction factor R:

$$T_0 = 2\pi \cdot \sqrt{m / k_0} \tag{3}$$

$$R = \frac{F_e}{F_y} \tag{4}$$

where k_0 is the initial stiffness of the system, F_e is the elastic design strength, and F_y is the yield strength dependent on the strength reduction factor R. The initial elastic stiffness and yield strength can be adjusted by altering the cross-sectional area and length using the known stress–strain relationship of the superelastic SMA element. The range of initial elastic period considered in this study was 0.3 s$\leq T_0 \leq$2.5 s, which is typical for 2- to 20-story steel braced frames. The values of the strength reduction factor R considered in this study are 2, 4, and 6.

The nonlinear time-history analyses of SDOF systems employed a suite of seismic ground motions developed by Somerville et al. (1997) for the FEMA project on steel moment-resisting frames. The suite contains 20 records, designated as LA 01–20, that correspond to design basis earthquakes (DBE) (such as a seismic hazard level corresponding to 10% probability of exceedance in a 50-year period) for downtown Los Angeles, California. These records were derived from fault-parallel and fault-normal orientations of 10 earthquake records, and then scaled in amplitude to meet the target design spectrum defined by NEHRP for site class D (firm soil) (Somerville et al. 1997). The epicentral distances of the records range from 1.2–36 km, whereas the scaling factors typically range from 0.84–3.2. After scaling, peak ground accelerations (PGA) range from 2.30–9.99 m/s^2, and the average PGA is 5.78 m/s^2.

4.2 Seismic response indices

The following response indices of SDOF systems were evaluated in the comparative study of the three aforementioned constitutive models for superelastic Nitinol wires:

a. Peak displacement ductility: $\mu = x_{\max} / x_y$, where x_y is the "yield" displacement that corresponds to the "yield" strain ε_y=0.9% for the superelastic Nitinol wires. The "yield"-like plateau in the superelastic Nitinol is caused by phase transformation, instead of plastic deformation. Thus, no damage accumulates as long as the element strain does not exceed 8%. Beyond 8%, a residual strain may occur after unloading due to plastic deformation. Therefore, 8% is assumed as the maximum recoverable strain level for the superelastic Nitinol wires. If the damage-free and self-

centering features of superelastic SMA element are desired under earthquakes, the ductility ratio μ must be limited to 9.

b. Peak acceleration: $a_{\max}$, acceleration response is an important indicator of the base shear caused by seismic loading and of the potential damage of acceleration-sensitive elements.

c. Normalized dissipated energy: $e_{dis} = \frac{E_{dis}}{\frac{1}{2}k_0 x_y^2}$, where E_{dis} is the total hysteretic energy dissipated by the superelastic SMA element. This index measures the energy-dissipating capacity predicted by different constitutive models.

4.3 Results and discussion

Fig. 5 depicts the statistical results of the three response indices for the SDOF system under the 20 seismic records. Each sub-figure plots nine curves, including the results calculated from the three constitutive models. Among the curves, the middle set represents the ensemble average for each response index, whereas the upper and lower sets represent one standard deviation each from the ensemble average. These values were calculated based on the structural responses to 20 earthquakes in the DBE suite. The three constitutive models provide a similar variation trend of the response indices with the changed initial period of the SDOF system. The average curves of the peak displacement ductility, $\mu_{\max}$, and peak absolute acceleration, $a_{\max}$, from the three constitutive models indicate a maximum difference of less than 8%. Similarly, only a slight difference is observed between the two curves that represent one standard deviation from the ensemble average. However, noticeable differences exist among the energy dissipation index curves from the three models. Compared with the TM model, the FS model tends to overestimate the energy dissipation capacity for all three levels of the strength reduction factor R, and the ensemble average error could reach 35% when R=2. Similarly compared with the TM model, the MW model provides a fairly close estimation of the energy dissipation capacity when R=2 and R=4, but provides a significant overestimation when R=6, especially for short periods during which the error between the ensemble average curves could reach 60%. The difference is larger between the curves that represent one standard deviation from the ensemble average. Systems with short periods have peak displacement

ductility ratios that likely exceed the limit of 9 when R=6. None of the three constitutive models is able to accurately predict the energy dissipation capacity of the superelastic SMA elements when μ>9; thus, these cases are excluded from Fig. 5.

Fig. 6 shows the relationship between the response indices predicted by the three constitutive models when R=4. In the sub-figures, each data point represents a response index result of an SDOF system with a specific period subjected to an individual seismic record. In a few cases, the displacement ductility demands exceed the limit of 9. Such cases were excluded from Fig. 6, because none of the three constitutive models is able to reproduce the complex hardening behavior of superelastic Nitinol wires beyond the 8% strain. In these figures, the dashed lines delineate the boundary associated with a 10% difference; that is, any data point outside the boundaries implies that the relative difference between the response indices from two constitutive models is greater than 10%. Fig. 6 depicts that the peak displacement ductility and peak absolute acceleration have relatively small differences, which are less than 10% in most cases. However, larger differences in energy dissipation could be observed among the three constitutive models, mainly due to the varying predictions on energy dissipation capacities (i.e., the enclosed area by the hysteresis). As mentioned earlier, the MW model overestimates energy dissipation in large strain cycles, whereas the FS model overestimates energy dissipation in all cycles (as shown in Fig. 3). Thus, in comparison with the TM model, the MW model leads to larger energy dissipation only in cases with large displacement responses, whereas the FS model tends to overestimate energy dissipation in most cases of seismic analyses.

Fig. 7 indicates the typical stress–strain curve of the superelastic SMA elements from the three constitutive models for the SDOF systems (R=4) subjected to the earthquake record LA09. The hysteretic loops in Figs. 7(a)–7(c) and 7(d)–7(f) were obtained for the SDOF systems with an initial period of 0.3 and 3.0 s, respectively. Both the MW and FS models are rate-independent and thus provide hysteretic loops with identical features (such as “yield” stress, “post-yield” stiffness, and energy dissipation capacity) for the two values of T_0. The TM model provides a slightly different hysteresis in the two stress–strain curves in terms of the unloading segment height and energy dissipation capacity. In Fig. 7(d), the

hysteretic loops slightly shift downwards. However, the substantial vertical shift of the hysteretic loops in Fig. 2 is not observed in Figs. 7(a) and 7(d). As discussed earlier, the hysteretic loops shift due to gradual changes in the zero-strain temperature. Large amplitude vibration leads to large temperature variation; however, structural response in large amplitude under strong earthquakes usually lasts for a limited number of cycles, which are insufficient to accumulate a considerable change of zero-strain temperature or to induce an apparent shift of hysteretic loops. For the two values of T_0, the TM model predicts a less than 4 ºC change in the zero-strain temperature, which induces the negligible shift of hysteretic loops [Fig. 7(d)]. In general, the three constitutive models provide highly similar hysteretic loops and seismic responses in the two cases. The noticeable difference in hysteresis is due to the different characteristic shapes of the three constitutive models, rather than the loading-rate effect.

The hysteretic loops slightly differ among cases with different initial periods. Therefore, replacing rate-dependent models with rate-independent constitutive models seems applicable for seismic analysis of structures with superelastic SMA elements. The results in Figs. 5 and 6 also suggest that the rate-dependent thermal effect of superelastic SMA elements has no significant effect on its dynamic behavior under earthquake loading. All three aforementioned constitutive models for superelastic Nitinol wires provide rather close estimations of the peak displacement ductility and peak absolute acceleration.

5. NONLINEAR DYNAMIC ANALYSIS OF THE MDOF SYSTEM

This section discusses a nonlinear seismic analysis of a three-story steel-braced frame equipped with SMA-based bracing elements. The aforementioned three constitutive models for superelastic Nitinol wires are used to simulate the structural response and examine the loading rate effect of superelastic SMAs in seismic analyses of a prototype structure.

5.1 Prototype building

Zhu and Zhang (2008) proposed a special SMA-based bracing element called self-centering friction damping brace (SFDB), with a mechanical configuration that is schematically illustrated in Fig. 8(b). Two steel parts, designated as Blocks “A” and “B,” are able to slide past each other along the frictional surface.

Stranded superelastic Nitinol wires are attached to the two moving parts using anchoring fixtures. The original design (Zhu and Zhang 2008) employed a predetermined friction force at the sliding surface to enhance energy dissipation and improve seismic performance. In this study, the friction at the sliding surface is set as zero to minimize its impact to the comparative study; thus, only the Nitinol elements contributed the brace force. Fig. 8(a) depicts the three-story SFDB frame selected as the prototype for the nonlinear time-history analyses. This concentrically braced steel frame was designed according to a displacement-based design methodology (Zhu 2007). The "yield" capacities of SFDBs were 1552, 1280, and 736 kN for the 1st–3rd story, respectively. In the SFDBs, the superelastic Nitinol wire strands had 0.75 m length for all the stories. Fig. 8(a) shows the sections of beams and columns, which are assumed to use Steel A992 Grade 50 with a yield stress of 344 MPa. Both the section and material types are commonly used in the US. The prototype building had first and second natural periods of 0.48 and 0.19 s, respectively.

5.2 Nonlinear time-history analyses

The nonlinear time-history analyses of this three-story prototype building with SFDBs used the computer program DRAIN-2DX (Prakash et al. 1993). Two suites of earthquake records developed by Somerville et al. (1997) were employed. In addition to the aforementioned DBE suite, the frequent earthquake (FE) suite that corresponds to 50% probability of exceedance in 50 years in Los Angeles was considered. The FE suite included only 18 records because the last pair was ignored for its excessive frame response beyond the modeling capability of all three constitutive models. The epicentral distances range from 1.2–107 km, and their PGAs after scaling range from 2.26–7.75 m/s^2. In the nonlinear time-history analysis, only one bay of the braced frame shown in Fig. 8(a) was modeled and analyzed. Element Type 2 in DRAIN-2DX, that is, the plastic-hinge beam-column element, modeled the steel beams and columns in the frame. Except for those at the roof, all beam-to-column connections were modeled as rigid connection to consider the effect of attached gusset plates. The ends of all braces were likewise assumed as frictionless pins. A rigid floor diaphragm was assumed; thus, all nodes on the same floor were constrained together in the horizontal direction. The global P-Δ effect was also considered in this analysis.

Three new elements in DRAIN-2DX were developed specifically for this study to simulate the hysteretic behaviors of SMA braces using the aforementioned three constitutive models.

5.3 Results and discussion

Figs. 9–11 show the results of nonlinear seismic analyses of the three-story SFDB frames using the three constitutive models for superelastic Nitinol wires. Fig. 9 depicts the peak inter-story drift ratios of the three-story SFDB frames subjected to the ground motions in the FE and DBE suites. The ensemble averages of the peak inter-story drift ratios for the TM, MW, and FS models are, respectively, 0.75%, 0.78%, and 0.65% in the FE suite, as well as 1.21%, 1.22%, and 1.08% in the DBE suite. Using the TM model results, the differences in the peak inter-story drift ratios between the MW and TM models are less than 17% under all 20 earthquakes in the DBE suite, and less than 7% under 16 out of the 20 earthquakes. The differences in peak inter-story drift ratios between the FS and TM models are slightly larger; the maximum difference is 21% in the DBE suite, and the difference is less than 10% in 12 earthquakes records.

The self-centering behavior of SMA cause the negligible residual inter-story drifts after earthquakes in the three-story SFDB frame models using all three constitutive models. With the given Nitinol wire length, the maximum recoverable strain of 8% corresponds to 2% inter-story drift ratio for the building. Therefore, whenever the transient story drift ratio exceeds 2%, residual deformation may occur in the superelastic Nitinol wires after earthquakes. The Nitinol wires would then require replacement. The three aforementioned constitutive models cannot accurately capture the complex strain hardening behavior beyond the 8% strain. As long as the peak inter-story drift ratios of the three-story SFDB frames are less than 2% under seismic ground motions, the SFDBs need no repairs, and the three constitutive models are considered valid for this study.

The effects of the three constitutive models on the seismic behavior of the SFDB frame could be better understood in Fig. 10. The typical time histories of its relative roof displacement and absolute roof acceleration are indicated under the LA18 record, which was derived from the ground motion recorded at the Sylmar station during the 1994 Northridge earthquake (Somerville et al. 1997). The three constitutive

models provide highly similar seismic response time histories and close peak values of the roof displacement and acceleration.

Fig. 11 indicates the statistical nonlinear seismic responses of the three-story SFDB frame under the FE suite. Figs. 11(a)–11(c) depict the distribution of the ensemble average of the peak relative displacements, peak absolute acceleration, and peak inter-story drift ratio along the height of the three-story SFDB frames, respectively. The ensemble average was calculated based on the 18 ground motions in the FE suite. Fig. 12 indicates the results under the DBE suite. All three constitutive models provide similar distribution patterns of the seismic responses. Under both the FE and DBE suites, the peak absolute acceleration and peak inter-story drift ratio along the height of the building produce fairly uniform distributions, and the peak displacement distribution is almost linear. The three models estimated a generally similar ensemble average of structural responses. Table 2 shows the ensemble averages and standard deviations of the peak inter-story drift, roof displacement, floor acceleration, and base shear under the FE and DBE earthquakes. The values were computed using the TM, MW, and FS models. Compared with the results of the TM model, the MW model predicted close seismic responses in terms of ensemble averages and standard deviations, whereas the FS model provided moderately different results, particularly in the peak floor accelerations. These findings suggest that the structural seismic behavior is not significantly affected by the loading rate dependence of the material properties of superelastic Nitinol wires. The relative differences indicated in Figs. 11–12 and in Table 2 are mainly due to the different hysteretic shapes (e.g., transition smoothness and enclosed area) defined by the three constitutive models. Figs 2 and 3 indicate that, in addition to rate dependence, these three models demonstrate different levels of agreement with experimental results. The apparent discrepancy in the hysteresis between the FS and TM models lead to a relatively large difference in the seismic response of the SFDB frames.

6. CONCLUSIONS

With their self-centering and excellent fatigue performance, SMAs such as Nitinol demonstrate high potential for seismic protection of civil engineering structures. Most SMA materials exhibit strain-rate-

dependent mechanical behavior. However, implementing a micromechanics-based strain-rate-dependent constitutive model in structural analysis and design is rather complicated and computationally demanding. This study examines the feasibility of replacing rate-dependent models with rate-independent constitutive models for superelastic SMA elements in the seismic time-history analyses of structures.

Three uniaxial constitutive models for superelastic SMA are considered: (i) the rate-dependent thermomechanical model (TM model) that captures the loading rate-induced thermal effect of SMAs and coincides with the experimental stress–strain relationship at various loading rates; (ii) the modified Wilde model (MW model); and (iii) the piecewise-linear flag-shaped model (FS model). Although the latter two are rate-independent phenomenological models, their parameters could be conveniently tuned based on experimental data from a series of uniaxial tensile tests of superelastic Nitinol wires. A cyclic tensile test program was conducted at various dynamic loading periods (0.25, 0.5, 2.0, and 10 s) and at quasi-static loading rate with 6% strain amplitude. In addition to the rate dependence, these three constitutive models offer slightly different features in the stress–strain curves of superelastic Nitinol wires, such as transition smoothness, energy dissipation capacity, and so on.

Based on the time-history analyses of SDOF systems with different initial periods and strength reduction factors, a parametric study evaluated the effect of constitutive models on seismic response. The parameters of the two rate-independent constitutive models were calibrated using experimental data at a strain rate that corresponds to seismic loading rates. A total of 20 DBE ground motions in Los Angeles were used to obtain the performance differences. The two rate-independent constitutive models provided peak displacement ductility ratios and accelerations highly similar to the rate-dependent thermomechanical model, whereas the three constitutive models indicated noticeable differences in energy dissipation. Additionally, the seismic behavior of a three-story prototype building equipped with special SMA-based damping devices, termed as self-centering friction damping brace (SFDB), was analyzed using the three constitutive models. Based on the predicted seismic responses of the prototype building, the loading rate induced a similarly insignificant thermal effect. The difference in hysteretic shapes induces larger discrepancies than the loading rate effect. Notably, the MW and FS model

parameters were calibrated according to the dynamic test results of Nitinol wires, although they are rate-independent models.

The similar seismic responses predicted by the three constitutive models indicate that the use of rate-independent constitutive models is applicable for superelastic SMA in the seismic analyses of structures, as long as the parameters of the rate-independent models are tuned to the dynamic test data of SMA elements. However, the use of more sophisticated thermomechanical constitutive models for SMA remains necessary when significant changes in environmental temperature are expected.

ACKNOWLEDGEMENTS

The authors are grateful for the financial support from the National Natural Science Foundation of China (Project No. 51208447) and the Hong Kong Polytechnic University (Project No. A-PJ15). Findings and opinions expressed here, however, are those of the authors alone, not necessarily the views of the sponsor.

REFERENCE

Aiken, I. D., Nims, D. K., Whittaker, A.S. and Kelly, J. M. (1993). "Testing of passive energy dissipation systems," *Earthquake Spectra*. 9(3): 335-370.

Andrawes, B. and DesRoches, R. (2005) "Unseating prevention for multiple frame bridges using superelastic devices." *Smart Mater. Struct.*, 14: S60-S67

Auricchio, F. and Sacco, E. (1999) "Modelling of the rate-dependent superelastic behavior of Shape-Memory Alloys," ECCM '99, European Conference on Computational Machanics, August 31-September 3, Munchen, Germany.

Auricchio, F., Fugazza, D. and DesRoches, R. (2006) "Numerical and experimental evaluation of the damping properties of shape-memory alloys." *Journal of Engineering Materials and Technology* **128** 312-319

Boyd, J. G. and Lagoudas, D. C. (1998) "A thermodynamic constitutive model for the shape memory materials part I: the monolithic shape memory alloys." *International Journal of Plasticity* **6** 805-842.

Casciati, F., Faravelli, L. and Al Saleh, R. (2009) "An SMA passive device proposed within the highway bridge benchmark," *Structural Control and Health Monitoring*, 16: 657-667.

Christopoulos, C., Filiatrault, A., and Folz, B. (2002). "Seismic response of self-centering hysteretic SDOF systems," *Earthquake Engineering and Structural Dynamics*, 31: 1131–1150.

Clark, P. W., Aiken, I. D., Kelly, J. M., Higashino, M. and Krumme, R.C. (1995) "Experimental and analytical studies of shape memory alloy dampers for structural control." In: Smart Structures and Materials 1995: Passive Damping, Proc. SPIE Vol. 2445, San Diego, CA.

DesRoches, R., McCormick, J., and Delemont, M. (2004). "Cyclic properties of superelastic shape memory alloy wires and bars," *ASCE Journal of Structural Engineering*, 130(1): 38-46.

Dolce, M. and Cardone, D. (2001). "Mechanical behavior of shape memory alloys for seismic applications 2. Austenite NiTi wires subjected to tension." *International Journal of Mechanical Sciences*, 43: 2657-2677.

Dolce, M., Cardone, D., and Marnetto, R. (2000). "Implementation and testing of passive control devices based on shape memory alloys." *Earthquake Engrg. Struct. Dyn,*, 29(7): 945-968

Dolce, M., Cardone, D., Ponzo F.C., Valente C. (2005). "Shaking table tests on reinforced concrete frames without and with passive control systems," *Earthquake Engineering and Structural Dynamics*, 34(14): 1687-1717.

Graesser, E.J., and Cozzarelli, F.A. (1991). "Shape-memory alloys as new materials for aseismic isolation." *ASCE J. Eng. Mech*., 117(11): 2590-2608.

Kim, K., Lim, J., Kim, J. and Lim, Y.M. (2008) "Simulation of material failure behavior under different loading rates using molecular dynamics", *Struct. Eng. Mech*. 30(2): 177-190.

Kožar, I. and Ožbolt, J. (2010) "Some aspects of Load-rate sensitivity in visco-elastic microplane material model", *Computers and Concrete, An International Journal*, 7(4): 317-329.

Liang, C. and Rogers, C.A. (1990) "One-dimensional thermomechanical constitutive relations for shape memory materials," *J. of Intell. Mater. Syst. and Struct*., 1: 207-234.

Liu, J.L., Zhu, S., Xu, Y.L. and Zhang, Y. (2011) "Displacement-based design approach for highway bridges with SMA isolators," *Smart Structures and Systems*, 8(2): 173-190.

Mao, C. and Li, H. (2005) "SMA-based smart damper/displacement transducer." Smart Structures and Materials 2005: Sensors and Smart structures Technologies for Civil, Mechanical and Aerospace Systems, Proc. of SPIE Vol. 5765, Bellingham, WA. pp: 442-452

McCormick, J., DesRoches, R., Fugazza, D. and Auricchio, F. (2006) "Seismic vibration control using superelastic shape memory alloys." *ASME J. Engineering Materials and Technology*, 128: 294-301.

NEHRP (2003) "Recommended provisions for seismic regulations for new buildings and other structures." FEMA No. 450. Federal Emergency Management Agency, Washington, DC, 2003.

Ozbulut, O.E., Hurlebaus, S. and DesRoches, R. (2011) "Seismic response control using shape memory alloys: a review" *Journal of Intelligent Material System and Structures*, 22: 1531-1549.

Padgett, J. E., DesRoches, R. and Ehlinger, R. (2010) "Experimental response modification of a four-span bridge retrofit with shape memory alloys," *Structural Control and Health Monitoring*, 32(3): 165-173.

Prahlad, H. and Chopra, I. (2003) "Development of a strain-rate dependent model for uniaxial loading of SMA wires." *J. Intell. Mater. Syst. Struct.* **14** 429-442

Prakash, V., Powell, G.H., and Campbell, S. (1993). "DRAIN-2DX: Base Program and User Guide." Report No. UCB/SES-93/17, University of California, Berkeley, CA.

Seo, C. Y. and Sause, R. (2005) "Ductility demands on self-centering systems under earthquake loading." *ACI Structural Journal*, 102(2): 275-285

Sommerville, P., et al. (1997). "Development of ground motion time histories for Phase 2 of the FEAM/SAC steel project," SAC Background document SAC/BD-91/04, SAC joint venture, Sacramento, California.

Whittaker, A.S., Krumme, R., Sweeney, S.C. and Hayes, J.R. (1995) "Structural control of building response using shape-memory alloys. Phase 1," Construction Engineering Research Lab (Army), Champaign, IL.

Wilde, K., Gardoni, P., and Fujino, Y. (2000). "Base isolation system with shape memory alloy device for elevated highway bridges," *Eng. Struct.*, 22(3): 222-229.

Zhu, S. and Zhang, Y (2006) "A shape memory alloy-based reusable hysteretic damper for seismic hazard mitigation." *Smart Mater. Struct.*, 16: 1603-1613.

Zhu, S. and Zhang, Y. (2007a). "Seismic behavior of self-centering braced frame buildings with reusable hysteretic damping brace." *Earthquake Engineering and Structural Dynamics*, 36: 1329-1346.

Zhu, S. and Zhang, Y. (2007b) "A thermomechanical constitutive model for superelastic SMA wire with Strain-rate dependency." *Smart Mater. Struct.*, 16: 1696-1707.

Zhu, S. and Zhang, Y. (2008). "Seismic analysis of concentrically braced frame systems with self-centering friction damping braces." *Journal of Structural Engineering*, 134(1): 121-131.

Zhu (2007) "Seismic behavior of framed structural systems with self-centering friction damping braces," Ph.D. dissertation, Department of civil and environmental engineering, Lehigh University, Bethlehem, PA, USA.

Table 1 Parameters of three constitutive models for superelastic Nitinol wires

	Parameter		Value	Parameter		Value
TM model	M_s	[°C]	-48	ε_l	[--]	0.03
	M_f	[°C]	-86	c_A	[MPa/K]	4.0
	A_s	[°C]	-42	c_M	[MPa/K]	3.5
	A_f	[°C]	-9	C_p	[J/(kg·K)]	600
	E_A	[GPa]	30	L	[J/kg]	22,000
	E_M	[GPa]	22	k	[W/K]	0.021
MW model	E_A	[GPa]	30	f_T	[--]	0.057
	E_M	[GPa]	21	a	[--]	200
	ε_m	[--]	0.06	c	[--]	0.6
	ε_1	[--]	0.043	n_1	[--]	3
	Y	[GPa]	290	n_2	[--]	0.5
	α	[--]	0.2			
FS model	E_A	[GPa]	30	α	[--]	0.17
	E_M	[GPa]	21	β	[--]	0.42
	σ_y	[MPa]	267	ε_M	[--]	0.052

Table 2 Ensemble average and standard deviation (in brackets) of seismic response of the 3-story SFDB frame under frequent earthquakes (FE) and design basis earthquakes (DBE)

			TM model	MW model	FS model
FE	Maximum story drift	(%)	0.60 (0.38)	0.59 (0.36)	0.52 (0.34)
	Roof displacement	(cm)	5.40 (2.99)	5.44 (3.12)	4.87 (2.79)
	Maximum acceleration	(m/s^2)	8.42 (3.35)	7.85 (3.01)	7.20 (2.57)
	Base shear	(kN)	2,845 (753)	2,702 (782)	2,655 (732)
DBE	Maximum story drift	(%)	1.21 (0.55)	1.22 (0.58)	1.08 (0.50)
	Roof displacement	(cm)	12.0 (5.78)	12.4 (6.13)	11.0 (5.40)
	Maximum acceleration	(m/s^2)	12.2 (5.3)	11.6 (4.4)	10.4 (3.6)
	Base shear	(kN)	4,568 (1,919)	4,470 (1,821)	4,174 (1,479)

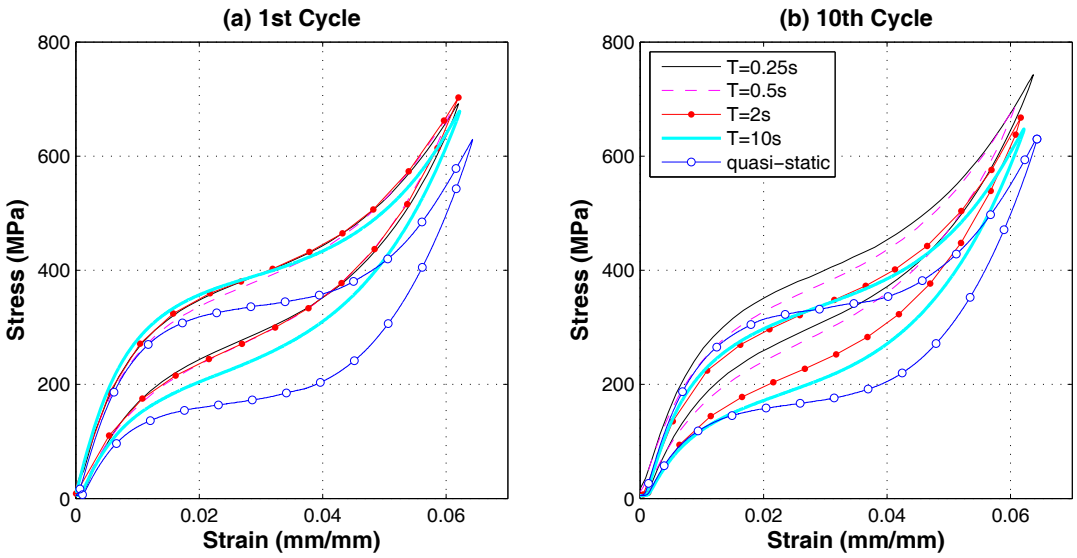

Figure 1. Stress-strain curves of Nitinol wires for 1st and 10th cycles under different loading rates

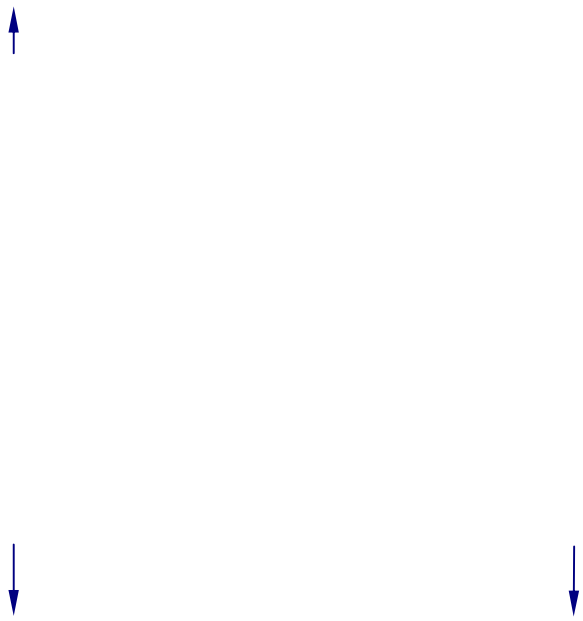

Figure 2. Stress-strain curves of superelastic Nitinol wires from the experiment data and from the TM model at various loading rates

(a) Modified Wilde model (b) Flag-shaped model

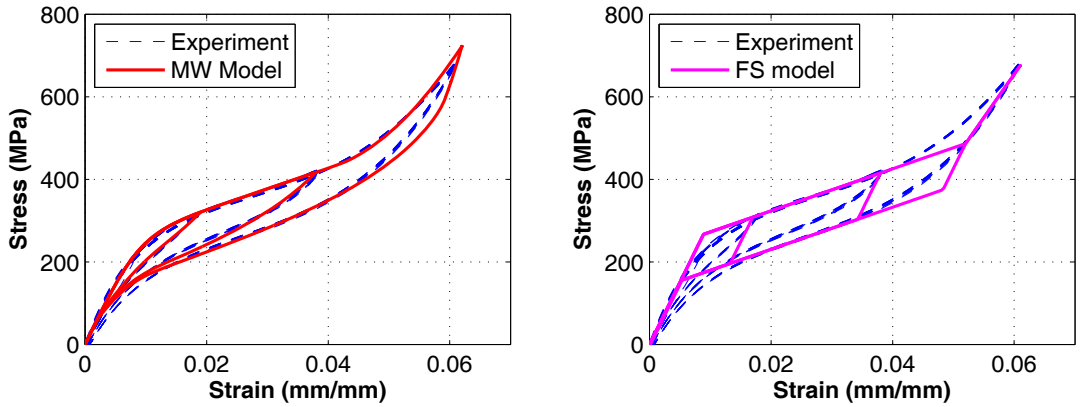

Figure 3. Stress-strain curves of superelastic Nitinol wires from experimental data (at loading period of 0.5 sec) and from the two rate-independent models

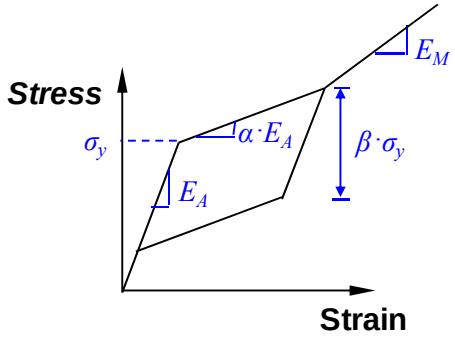

Figure 4. Typical flag-shaped hysteretic loop for superelastic Nitinol wires

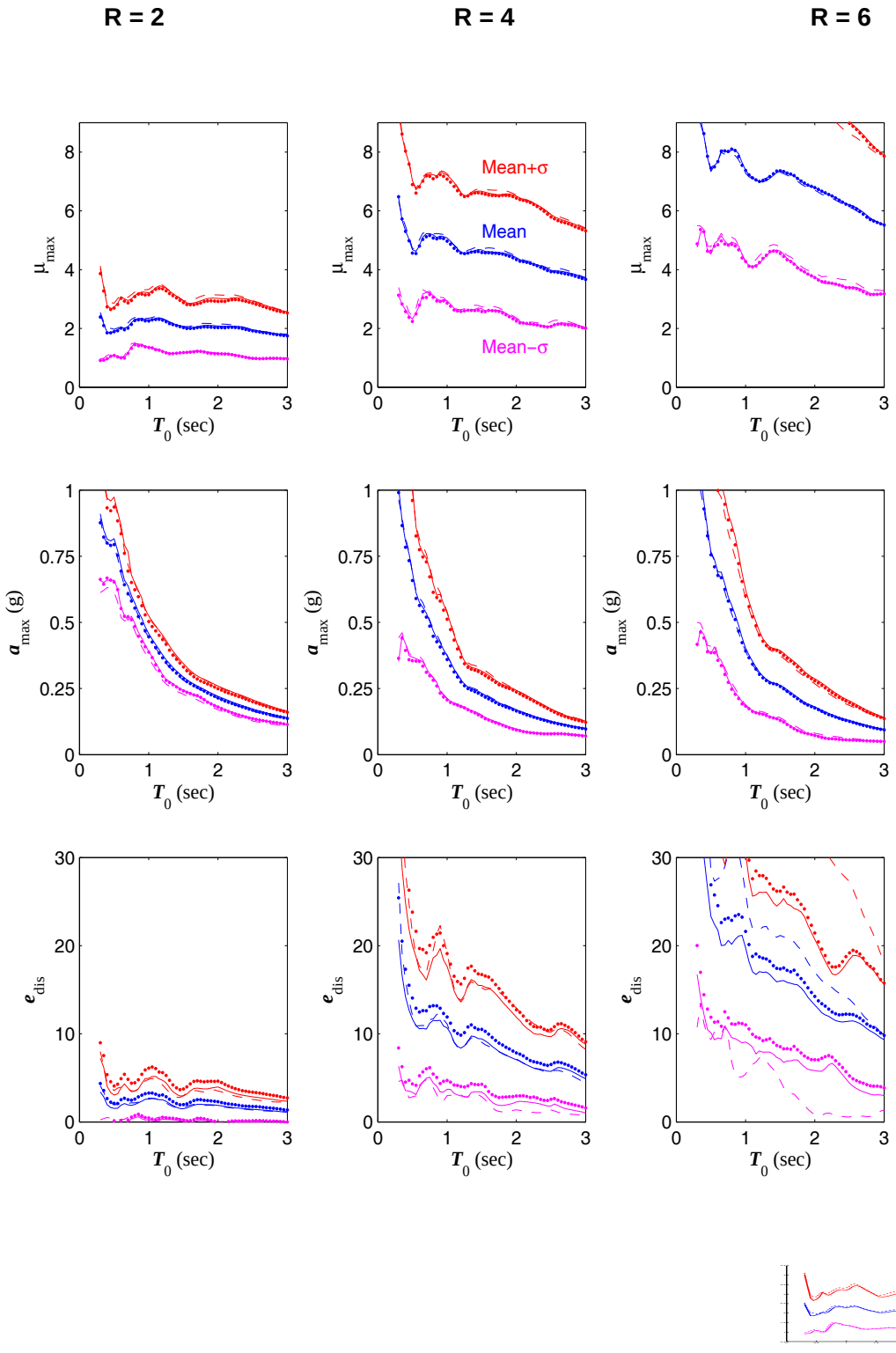

Figure 5. Statistical results of the response indices for SDOF system

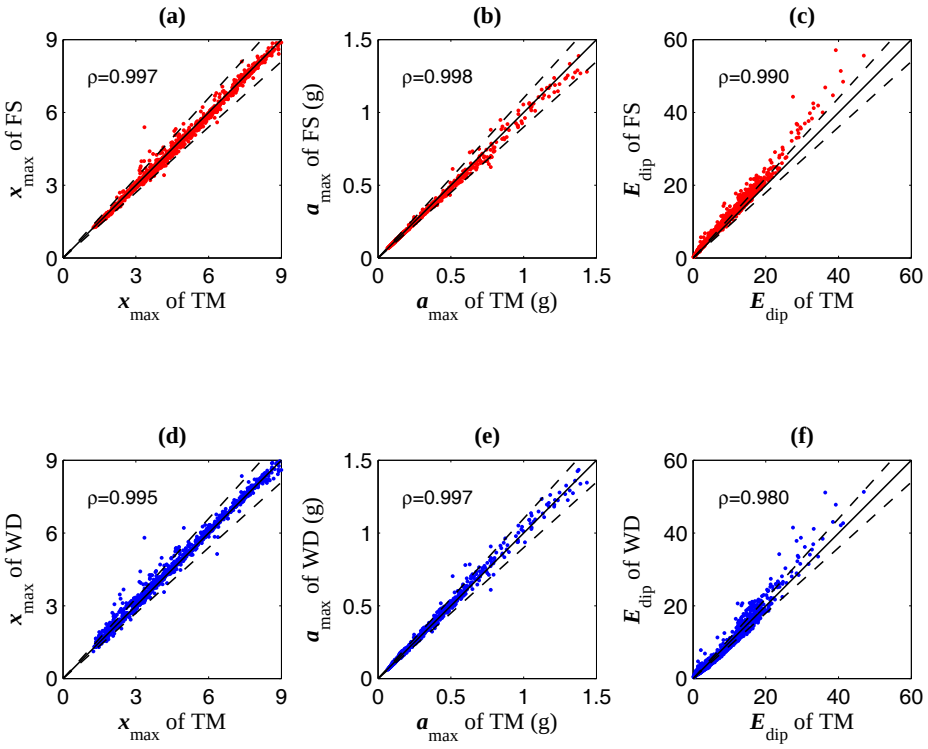

Figure 6. Comparison of response indices for R=4: (a), (b) and (c) - FS model vs. TM model; (d), (e) and (f) - WD model vs. TM model

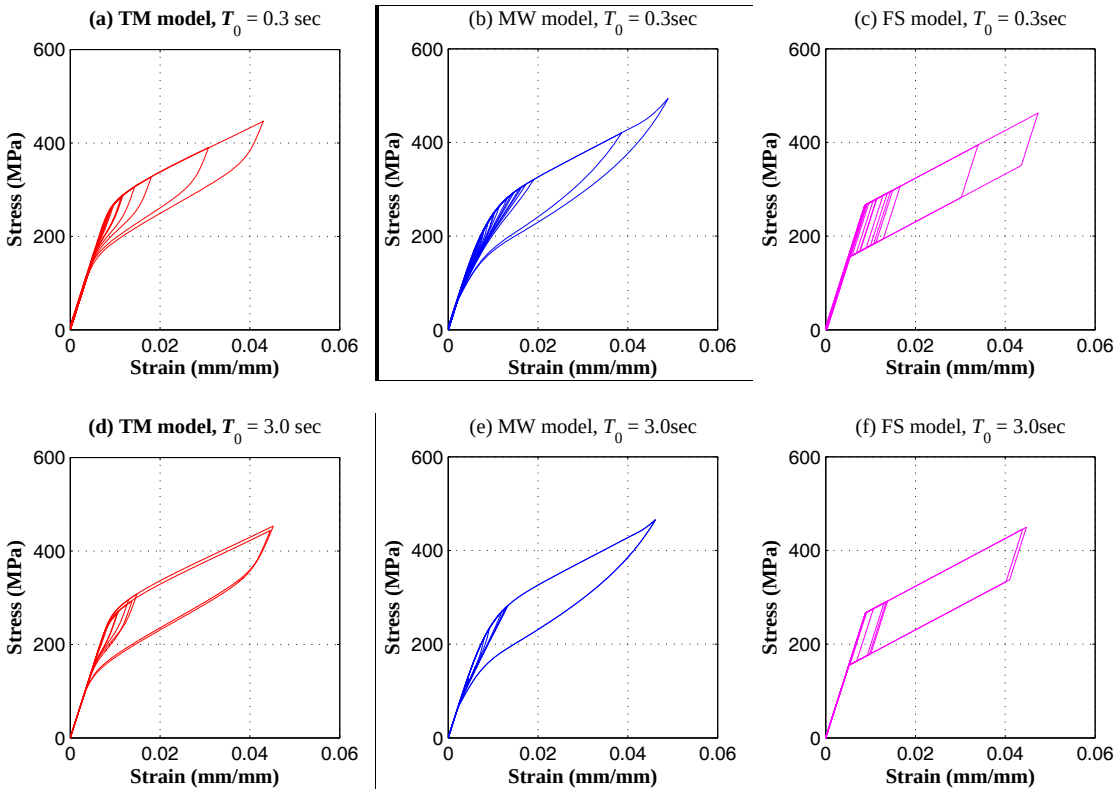

Figure 7. Typical stress-strain curves of superelastic Nitinol elements (R = 4) under seismic record LA09

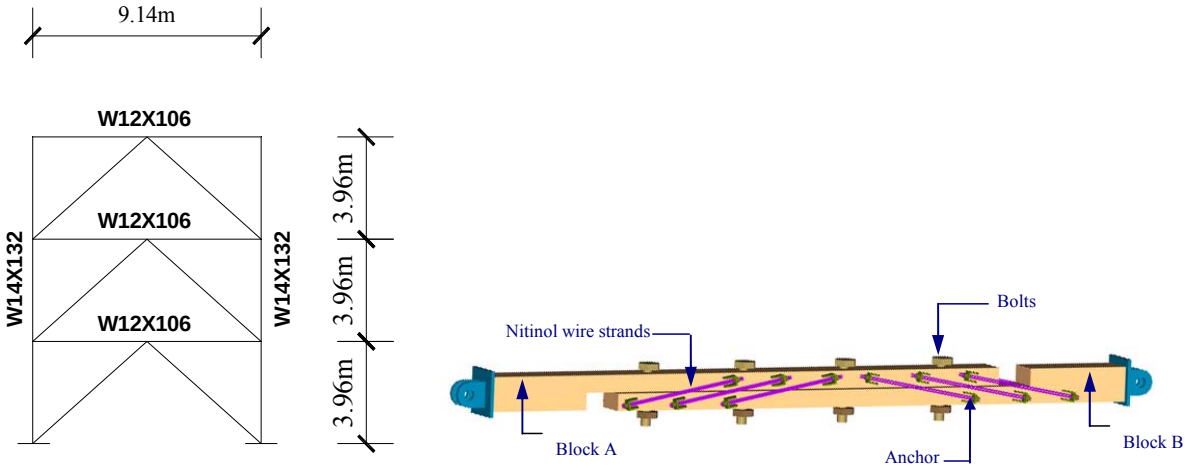

(a) 3-story prototype frame (b) Mechanical configuration of SFDB

Figure 8. Configuration of 3-story braced frame and SFDB

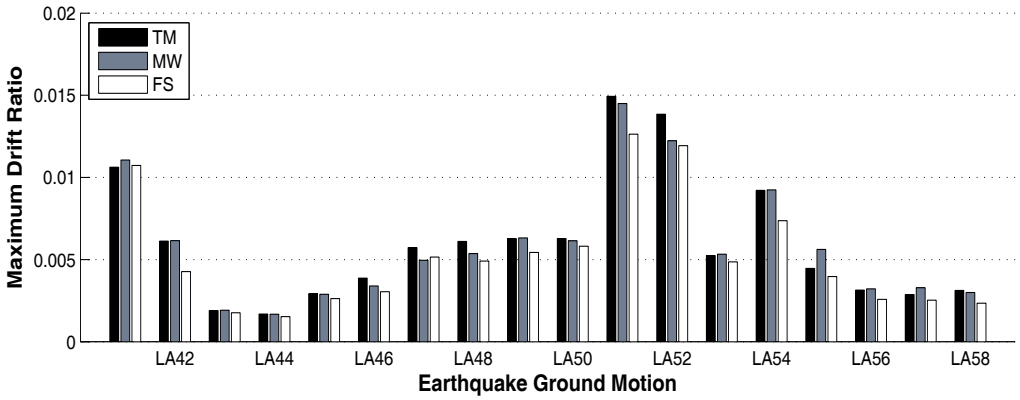

(a) Under FE ground motions

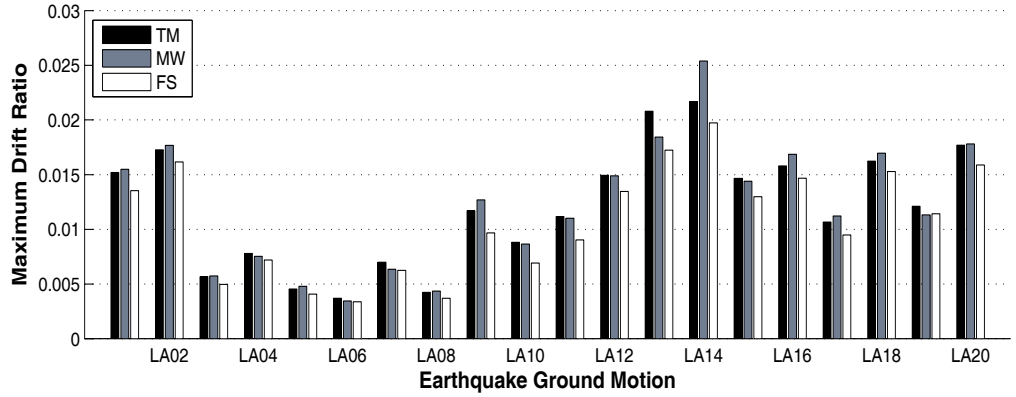

(b) Under DBE ground motions

Figure 9. Peak inter-story drift ratios for the 3-story SFDB frame

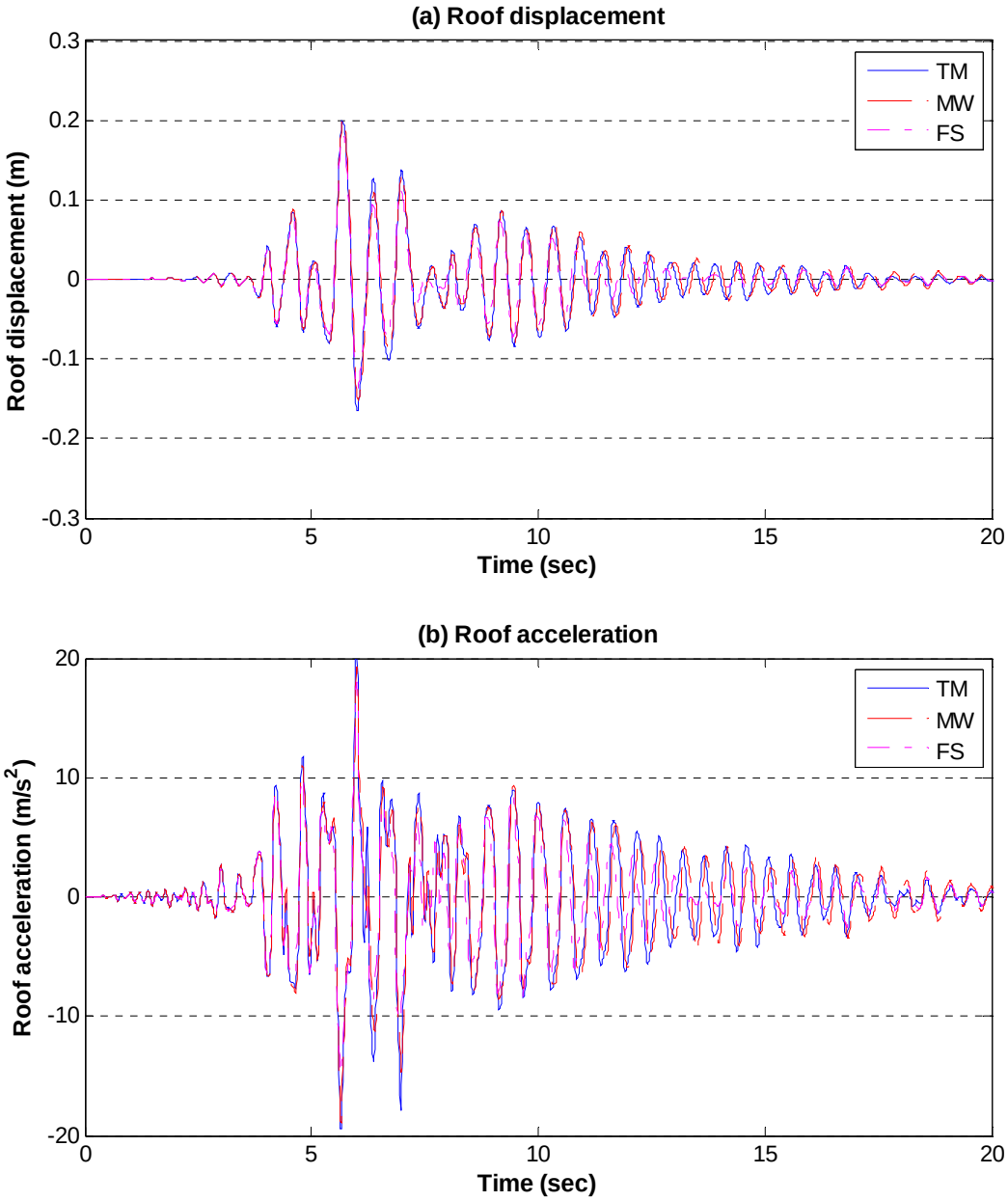

Figure 10. Time history response of the 3-story SFDB frame under ground motion LA13

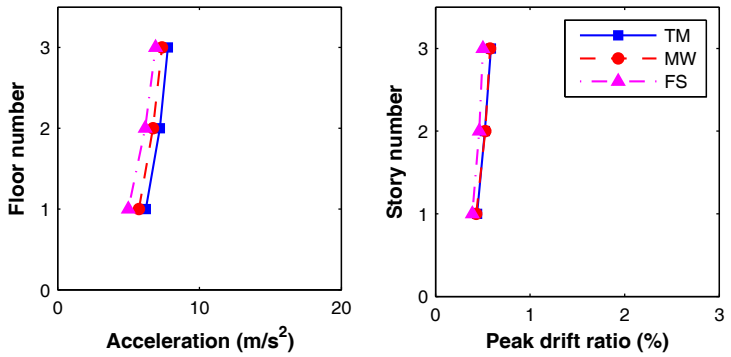

Figure 11. Ensemble average of seismic response of the 3-story SFDB frame under FE ground motions: (a) Peak displacement; (b) Peak acceleration; (c) Peak inter-story drift ratio

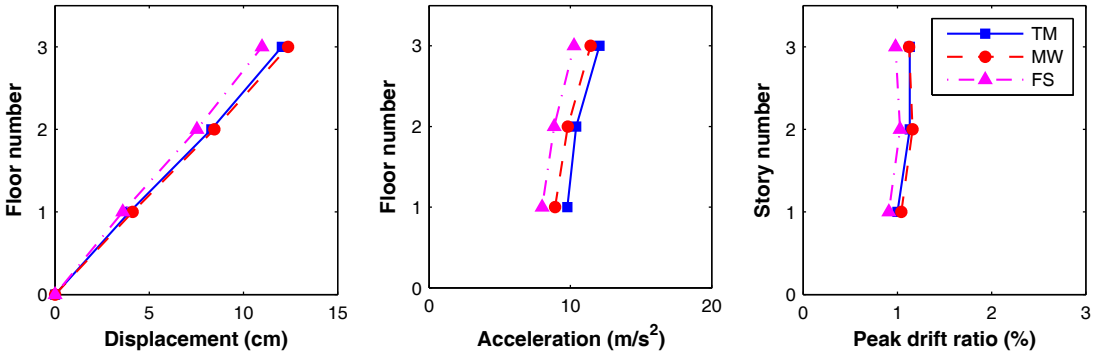

Figure 12. Ensemble average of seismic response of the 3-story SFDB frame under DBE ground motions: (a) Peak displacement; (b) Peak acceleration; (c) Peak inter-story drift ratio